# A new Delaunay triangulation-based approach to characterize the pore network in granular materials

Ngoc-Son Nguyen, Habib Taha, Didier Marot

# A new Delaunay triangulation based approach to characterize the pore network in granular materials

**Article** *in* Acta Geotechnica · July 2021

DOI: 10.1007/s11440-021-01157-1



**3 authors**, including:

Ngoc-Son Nguyen
University of Nantes
**24** PUBLICATIONS **181** CITATIONS
SEE PROFILE

Didier Marot
University of Nantes
**102** PUBLICATIONS **1,040** CITATIONS
SEE PROFILE

**Noname manuscript No.**
(will be inserted by the editor)

# A new Delaunay triangulation based approach to characterize the pore network in granular materials

**Ngoc-Son Nguyen · Habib Taha · Didier Marot**

Received: date / Accepted: date

**Abstract** The ability of granular materials to retain fine particles transported within their void space by seepage flow depends strongly on the geometric characteristics of their pore network (pore sizes and constriction sizes). Hence, characterizing the pore network of a granular assembly obtained by means of a micro-tomography scanning or a numerical discrete simulation is of great importance in assessment of its filtration efficiency. Here we determine characteristics of the pore network of virtual samples composed of spherical particles simulated by using the DEM. A new criterion is proposed to merge neighboring tetrahedra issued from the weighted Delaunay triangulation. To do so, we extend the concept of inscribed void sphere, initially defined for each tetrahedron, to each polyhedral sub-domain constituted of merged tetrahedra. This inscribed void sphere fits the best the void space within the sub-domain. Flat tetrahedra are first eliminated by a primary merging procedure taking into account two basic geometric conditions required for each pore. Adjacent sub-domains are then merged depending on the level of overlap between their inscribed void spheres. The pore size distributions (PSD) and constriction size distributions (CSD) of granular samples with different grain size distributions (GSD) obtained with the new merging criterion are compared to those given by two other criteria often used in the literature. The new criterion allows us to reduce greatly the inherent subjectivity in characterizing the granular pore network and to remediate the drawbacks of the two considered criteria in the literature. Moreover, CSDs given by these different criteria tend to converge for gap-graded and widely graded materials. The CSDs obtained with the new merging criterion are used to estimate the controlling constriction sizes $D_c^*$ of the considered samples and the estimated values of $D_c^*$ are compared to Kenney and Lau's empirical rule.

Ngoc-Son Nguyen E-mail: ngocson.nguyen@univ-nantes.fr · Habib Taha E-mail: habib.taha@etu.univ-nantes.fr · Didier Marot E-mail: didier.marot@univ-nantes.fr
GeM Institute, University of Nantes, 58 rue Michel Ange, BP 420, 44606, Saint-Nazaire Cedex, France

**Keywords** Granular materials · DEM · Pore network · Delaunay triangulation · Merging criterion

## 1 Introduction

Hydraulic earth structures such as dikes and embankment dams are built to prevent flooding, provide hydropower, store water for drinking or irrigation, etc. However, these structures can suffer from instabilities due to internal erosion which is one of the main causes of their failures. Granular filters, which are designed as part of a drainage system, play an important role in halting internal erosion by trapping eroded particles. Suffusion is a particular form of internal erosion for which fine particles of a suffusive soil are detached and transported through its pore network. It is generally accepted that (i) a granular soil possesses a primary fabric of particles which supports mainly imposed stresses; (ii) the pores of the primary fabric contain loose particles which can be detached by water flow; and (iii) the primary fabric acts as a granular filter to prevent migration of loose particles [12]. Thus, the susceptibility of a granular soil to suffusion depends strongly on the ability of its primary fabric to retain its own loose particles. The geometry of the pore network within a granular filter, in particular, the sizes of constrictions in comparison with the sizes of the base particles is the most important factor that influences the efficiency of the filter, and thus the suffusion susceptibility of the granular soil in question [11]. Nevertheless, these properties are usually assessed by particle size gradation based criteria which do not consider the geometry of the pore network.

With the purpose to take into consideration the geometry of the pore network of a granular filter when assessing its performance, the constriction size distribution (CSD) has been used to estimate the controlling constriction size [10,24] or to distribute sizes of the tubes in a regular cubic pore network [23]. The latter, which is composed of a regular cubic array of pores connected by tubes representing constrictions, has been used in particle-based transport models to assess the filtration efficiency [18,28]. Silveira [30] was a pioneer in developing a probabilistic method to estimate the CSD of a granular filter by assuming that constrictions are formed by three and four solid spheres mutually in contact for the densest and loosest states, respectively. This method has been subsequently improved in several works [18,22,24]. The probabilistic method offers a quick way to estimate the CSD; nevertheless, its accuracy needs to be further studied. Numerical methods have been developed as alternative tools to determine the CSD of granular materials.

Nowadays, high-resolution images of a physical granular packing can be obtained by using the micro-computerized-tomography ($\mu$CT) scanning technology. Several numerical methods have been developed to extract the pore network from its image such as maximal ball method [1,7,29] and Voronoi-based method [9,17]. These methods were proved to be capable of characterizing realistic pore spaces of soils with irregular particle shapes and complex

arrangements. However, $\mu$CT scanner is very expensive; in addition, scanning a soil specimen results in a very big data which needs to be handled by efficient algorithms and supercomputers.

Instead of scanning real soil specimens, the discrete element method (DEM) can be used to create virtual soil specimens. To gain the computation time, most of virtual materials simulated with the DEM are composed of spherical particles. However, one can consider more complex particle shapes such as polyhedra, ellipsoids or clusters of overlapping spheres. Das [6] showed that complex particle shapes of a real soil can be accurately modeled by clustering overlapping spheres. The DEM allows us to generate quickly a virtual granular sample according to a given grain size distribution (GSD); and the sample data is of reasonable size compared to that given by $\mu$CT scanning. For instance, a sample of particles modeled by clusters of overlapping spheres is fully described by the centers and radii of the spheres. It should be noted that the characteristics of a granular pore space depend on several parameters, primarily on the GSD and on the compactness. Spherical particles allow us to take into account these two primary parameters despite their simplicity. Moreover, Delaunay triangulation can be used for spherical particles, offering great advantages in defining pores and constrictions. Therefore, several methods based on Delaunay triangulation have been proposed; they can be classified into two main approaches: *interstitial void* based methods [2,8,15,16,21,22,25,27,31, 34] and *contact* based method [20]. For both approaches, the whole volume of a granular sample is subdivided into a set of tetrahedra. Each tetrahedron joins the centers of four neighboring particles in the first approach, while it joins four neighboring contact points between particles in the second one. By doing so, the pore space is artificially over-subdivided so adjacent tetrahedra need to be merged according to a certain criterion. Thus, merging criteria are crucial in these approaches to obtain an accurate description of the pore space.

Most merging criteria proposed for void based methods rely on the concept of *inscribed void spheres* defined for each tetrahedron. Overlap between two adjacent inscribed void spheres is considered as a degree of correlation between the two corresponding adjacent tetrahedra. Al-Raoush et al. [2] proposed to merge two adjacent tetrahedra if the center of an inscribed void sphere lies within the neighboring one, *i.e.* a partial overlap between two adjacent inscribed void spheres is allowed. On the contrary, Sufian et al. [31] merged every couple of adjacent tetrahedra if their inscribed void spheres overlap by any amount. Shire and O'Sullivan [27] used a user-specified value for the admissible overlap between two adjacent inscribed spheres. It is worth mentioning that the choice of this admissible overlap is subjective; and the pore size distribution (PSD) and the CSD are strongly dependent on this value. It seems logical to choose a zero admissible overlap as adopted by Sufian et al. [31]. However, this zero threshold value results in over-merging of tetrahedra, thus in formation of pores of complex shapes, *i.e.* they correspond actually to ducts (chains of pores) rather than single pores. To avoid this over-merging of tetrahedra, Reboul et al. [21,22] introduced two merging levels, according to which merging can only span from a central tetrahedron to its nearest neigh-

bors (level $L_1$) and to its next nearest neighbors (level $L_2$). The choice of a merging level is not obvious and has a great influence on the obtained PSD and CSD.

As stated by Shire and O'Sullivan [27], the void space within granular materials is a complex network where adjacent pores are interconnected. For such a continuous void space, any attempt to subdivide it into single pores suffers from an inherent subjectivity. Nevertheless, it is important to minimize the impact of this subjectivity when characterizing the granular pore network and give a better confidence when using the obtained characteristics. This is the main motivation of the work presented in this paper. We adopt a void based approach and present a new criterion to merge neighboring tetrahedra. The concept of inscribed void spheres defined for each tetrahedron is generalized to polyhedral sub-domains, each of which is composed of a cluster of neighboring tetrahedra. This new criterion makes use of a user-specified value; nevertheless, the subjectivity in choosing this value is greatly reduced by the new criterion.

We first present virtual granular samples used for the void partitioning. Then, a brief literature review focused on the two void based methods of Shire and O'Sullivan [27] and of Reboul et al. [21,22] is presented; and their advantages and drawbacks are discussed. Next, we present a new merging criterion to define pores and constrictions. In Section 5, results obtained with the new criterion are compared to those given by the two other criteria mentioned above. Finally, CSDs obtained with the developed criterion are used to estimate the controlling constriction sizes $D_c^*$ of the simulated samples and the obtained results are discussed in Section 6.

## 2 Virtual granular samples

Six virtual samples composed of spherical particles are simulated by using the DEM open-source software YADE [33]. Linear force-displacement laws combined with Coulomb friction law are used for the normal and tangential interactions at each contact between particles. The input parameters needed for the performed numerical simulations are: particle mass density $\rho = 2600$ kg/m$^3$, particle normal stiffness $k_n/D = 250$ MPa ($D$ is the particle diameter), particle tangential stiffness $k_t/k_n = 0.5$, and the fiction angle $\varphi$ whose value is chosen depending on the target compactness.

Three GSDs are considered: uniformly graded (UG), gap-graded (GG) and widely graded (WG) as shown in Figure 1. The first and second GSDs were considered by Seblany et al. [25]. To create a sample, particles matching a given GSD are first generated into a cube composed of six rigid walls. At this stage, each particle diameter is reduced by a factor of 2.0. Particles are then progressively expanded to reach the target GSD. After that, the box dimensions are slowly reduced until the stresses $\sigma_i$ ($i = 1, 2, 3$) reach a confining stress of 100 kPa. To obtain dense samples, the friction angle $\varphi$ is set to 0 to facilitate arrangement of particles during the compaction process, while it is set to 35° to obtain loose samples. The gravity is set to zero during this

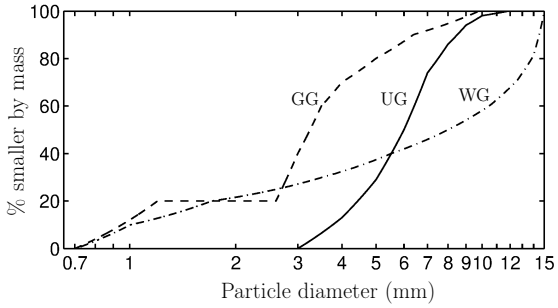


**Fig. 1** GSDs of the considered virtual samples: uniformly graded (UG), gap-graded (GG) and widely graded (WG).

generation process to avoid segregation of particles. Indeed, this phenomenon occurred for the widely-graded materials considered here when particles were deposited under gravity. Table 1 presents some gradation properties, the number of particles and the porosity $n$ of the six samples considered in the current study. It is worth mentioning that the three GSDs considered here are stable according to Kenney and Lau's criterion [12,13] and Chang and Zhang's criterion [4]. In the following, each sample is named by its GSD (UG, GG or WG) followed by letter L for the loose state and D for the dense state.

| Sample | Gradation properties | Number of particles | Porosity $n$ | |
|---|---|---|---|---|
| | | | Loose state | Dense state |
| UG | $C_\mathrm{u} = 1.7$ | 6 000 | 0.41 | 0.36 |
| GG | $C_\mathrm{u} = 3.7$, $G_\mathrm{r} = 2.2$ $f_\mathrm{c} = 20\%$ | 25 000 | 0.31 | 0.26 |
| WG | $C_\mathrm{u} = 10.4$, $(H/F)_\mathrm{min} = 1.3$ for $F < 20\%$ | 30 000 | 0.23 | 0.19 |

**Table 1** Gradation properties (coefficient of uniformity $C_\mathrm{u}$, gap ratio $G_\mathrm{r}$, fine content $f_\mathrm{c}$ and ratio $(H/F)_\mathrm{min}$), number of particles, and porosity $n$ of the six simulated samples. $F$ and $H$ are the mass fractions of particles smaller than a size $d$ and between sizes $d$ and $4d$, respectively.

The above sample generation procedure without gravity results in a particular fraction of particles, namely *rattlers*, that are floating within the pores and have no contact with their neighbors. Although the rattlers are the most likely to be detached by the water flow, removing all of them does not represent accurately the internal state of an eroded soil. As the main purpose of this paper is to compare different approaches used to determine the characteristics of the pore space formed by a given set of solid spheres, the rattlers are not discarded in the following comparisons. The influence of these rattlers on characteristics of the pore network is studied in Section 6.

## 3 Literature review of void based methods

A void based method subdivides first the whole volume of a granular assembly into tetrahedra, each of which joins the centers of four neighboring particles, by using the weighted Delaunay triangulation, also known as the regular triangulation. This triangulation technique, implemented in the CGAL library [32], is applied to a set of *weighted* points $(C_p,\ w_p)$ which can be seen as spheres of center $C_p$ and radius $R = \sqrt{w_p}$. The treatment proposed by Catalano [3] is used to ensure a relevant tessellation near the boundaries composed of the six rigid walls. It consists in considering each rigid wall as a fictitious sphere of infinite radius that is placed to be tangent to the assembly. By doing so, spheres near a rigid wall are all connected to the corresponding fictitious sphere by fictitious branches (dotted lines in Figure 2); therefore degenerated tetrahedra near the boundaries can be avoided. Once the weighted Delaunay triangulation is performed, all fictitious branches are removed from the Delaunay network. All spheres that are connected to fictitious boundary spheres by fictitious branches are considered to be near the boundaries (dashed spheres in Figure 2). All the tetrahedra and pores near the boundaries (those contain at least one sphere near the boundaries) are discarded from the following analyses.

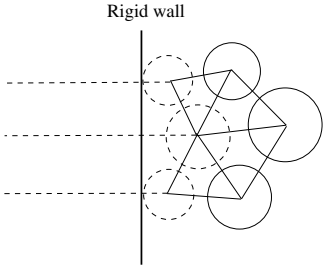


**Fig. 2** Illustration of the technique used to avoid degenerated tetrahedra near a rigid wall. Dashed spheres near the rigid wall are connected to the fictitious one by dashed branches.

An inscribed void sphere is then identified for each tetrahedron. This is the sphere that is tangent to all the four solid spheres joined by the tetrahedron under consideration. The center $\boldsymbol{X}$ and radius $R$ of the inscribed void sphere can be uniquely identified by solving a system of four non-linear equations $d_i(\boldsymbol{X}, R) = 0\ \ \forall i = 1,\ 2,\ 3,\ 4$ where $d_i$ is the distance between the void sphere and each solid sphere $i$. For very flat tetrahedra, this system of equations might adopt no solution. In this case, the inscribed void sphere can be identified by a minimization problem. The inscribed void sphere of a given tetrahedron might intersect solid spheres in the vicinity. In this case, this inscribed void sphere must be replaced by the largest void sphere that can fit within the void space between the solid spheres joined by the tetrahedron under consideration and the intersected adjacent solid ones. This largest inscribed void sphere can be

identified by the optimization algorithms proposed by Al-Raoush et al. [2] and by Sufian et al. [31].

The inscribed void spheres of a couple of adjacent tetrahedra can overlap, and this overlap can be considered as a degree of interconnection between the two tetrahedra under consideration. A criterion is then needed to assess this degree of interconnection. Shire and O'Sullivan [27] considered a relative overlap $\gamma$ between two adjacent inscribed void spheres defined as $\gamma = \delta / \min(d_i, d_j)$ where $\delta$ is the overlap between them (see Figure 3); $d_i$ and $d_j$ are their diameters. The authors proposed to use a user-specified value $\gamma^{\text{th}} \in [0,\ 1]$ for the admissible overlap. Any couple of adjacent tetrahedra for which the relative overlap $\gamma$ is greater than the user-specified value $\gamma^{\text{th}}$ are considered to be interconnected, and are then merged together. The choice of $\gamma^{\text{th}}$ is subjective. Al-Raoush et al. [2] merged two adjacent tetrahedra if the center of an inscribed void sphere lies within the other one, *i.e.* $\gamma^{\text{th}} = 0.5$. On the other hand, Sufian et al. [31] merged two adjacent tetrahedra if their inscribed spheres overlap by any amount, *i.e.* $\gamma^{\text{th}} = 0$.

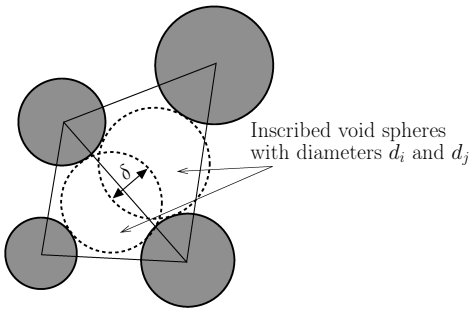


**Fig. 3** 2D illustration of the overlap $\delta$ between the inscribed void spheres of two adjacent tetrahedra.

Let us vary the user-specified value $\gamma^{\text{th}}$ from 0.5 to 0 and then show how the pore size distribution (PSD) obtained with this criterion is sensitive to $\gamma^{\text{th}}$. The size of a pore is defined as the diameter $D^*$ of an equivalent void sphere whose volume is equal to the volume of the pore under consideration. Figure 4.a shows the PSDs in terms of void volume obtained for the UGL sample with different values of $\gamma^{\text{th}}$. The curve $\text{L}_0$ corresponds to the pores defined by each tetrahedron given by the Delaunay triangulation. It can be seen that the PSD given by this merging criterion is very sensitive to the user-specified value $\gamma^{\text{th}}$. It is worth mentioning that the pores are very heterogeneous in size, and an important number of small pores are formed by single tetrahedra whatever the value of $\gamma^{\text{th}}$. For instance, 55% by number of the pores obtained with $\gamma^{\text{th}} = 0$ are formed by single tetrahedra; however, they occupy only 12% of the void volume of the sample. Therefore, the dependency of the PSD upon $\gamma^{\text{th}}$ is better seen when plotting the distribution in terms of volume of pores than when plotting the distribution in terms of number of pores. It is logical

to choose $\gamma^{\text{th}} = 0$; however, this value leads to formation of many big pores: 20% of the void volume of the sample is actually occupied by very big pores, each of which is formed by more than 20 merged tetrahedra. This value of $\gamma^{\text{th}}$ tends to over-merge tetrahedra and many resulting pores represent poorly single pores: they correspond to rather chains of pores as illustrated in Figure 4.b.

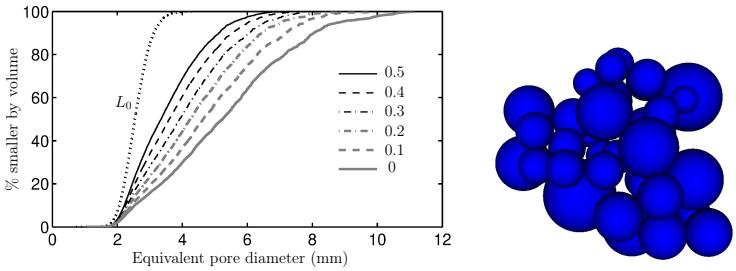


**Fig. 4** (a) PSDs given by the criterion of Shire and O'Sullivan for the UGL sample with $\gamma^{\text{th}}$ varied from 0.5 to 0, and (b) a pore composed of 66 tetrahedra is given by $\gamma^{\text{th}} = 0$.

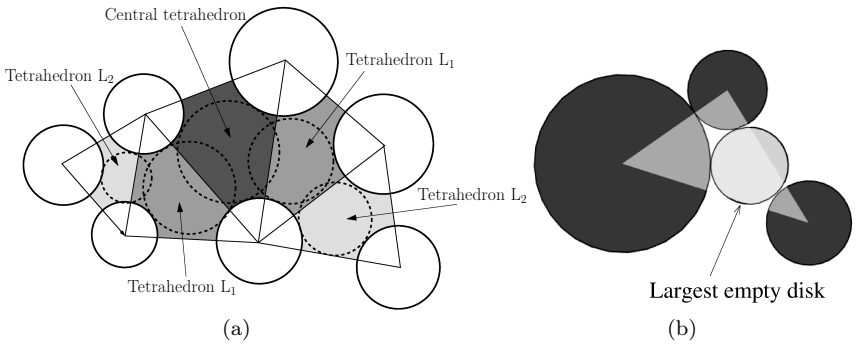


**Fig. 5** (a) Illustration of adjacent tetrahedra of levels $L_1$ and $L_2$ according to Reboul et al. [21], and (b) the largest empty disk inscribed between three solid disks of a triangular face.

Reboul et al. [21,22] defined two merging levels $L_1$ and $L_2$ to avoid over-merging of tetrahedra. The $L_1$ level allows the merging process to go from a given tetrahedron, which is selected as the central one, to only its direct neighbors (tetrahedra $L_1$ in Figure 5.a), while the $L_2$ level extends the merging process to the next nearest neighbors (tetrahedra $L_2$ in Figure 5.a, which are the neighbors of the tetrahedra $L_1$). It should be noted that merging two adjacent tetrahedra is conditioned by an overlap by any amount between their inscribed void spheres ($\gamma^{\text{th}} = 0$). By doing so, the pore size is limited to five

and seventeen tetrahedra according to the levels $L_1$ and $L_2$, respectively. Seblany et al. [25] proposed to eliminate tetrahedra of undesirable shapes (flat tetrahedra having negligible volumes) which are artifacts of the weighted Delaunay triangulation before applying the levels $L_1$ and $L_2$. These flat tetrahedra correspond to two cases where (i) a couple of adjacent tetrahedra have their inscribed spheres almost superimposed or (ii) they share such a flat triangular face that the diameter of their common constriction is bigger than the diameters of their inscribed spheres. The constriction size was defined as the diameter of the largest empty disk that is tangent to the three solid disks on their common triangular face [22] (see Figure 5.b). The authors introduced a level $L'_0$ to eliminate these degenerated configurations by merging all couples of adjacent tetrahedra matching the two undesirable cases mentioned above. Moreover, they merged the tetrahedra in descending order of the diameter of their inscribed void sphere. In the following, these modifications proposed by Seblany et al. are taken into consideration in the criteria $L_1$ and $L_2$ of Reboul et al.

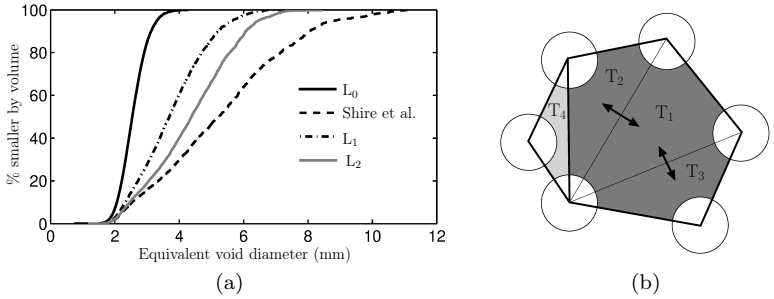


**Fig. 6** (a) PSDs given by the merging levels $L_1$ and $L_2$ of Reboul et al. for the UGL sample, compared to that given by the criterion of Shire and O'Sullivan with $\gamma^{\text{th}} = 0$. (b) A 2D single pore is subdivided into several entities by the $L_1$ criterion.

Figure 6.a shows the PSDs obtained for the UGL sample by using the merging criteria $L_1$ and $L_2$. It is shown that these criteria result in actually fewer pores of big sizes than the criterion of Shire and O'Sullivan with $\gamma^{\text{th}} = 0$. In addition, they give quite different PSDs. It should be noted that this difference is much less noticeable if the PSDs in terms of number of pores are plotted as shown by Reboul et al. [21]. The criterion $L_2$ is actually effective for 40% by number of the pores identified by the criterion $L_1$ (the biggest ones); however, these pores occupy 76% of the total void volume. Reboul et al. recommended to use the criterion $L_1$ as some complex entities are obtained with the criterion $L_2$, which represent poorly single pores. Nevertheless, as the pore size is limited to five tetrahedra, the criterion $L_1$ tends to subdivide pores composed of more than five tetrahedra into several smaller entities; and some entities represent inaccurately single pores. Figure 6.b illustrates a 2D pore composed of four triangles. According to the criterion $L_1$, the triangle

$T_1$ is chosen as the central one and its two direct neighbors $T_2$ and $T_3$ are merged to $T_1$ to form an entity, leaving the triangle $T_4$ alone which cannot be considered as a single pore. For such a case, the merging should be extended to the level $L_2$ to obtain a single pore.

As shown previously, the criterion of Shire and O'Sullivan gives PSDs very sensitive to the user-specified value $\gamma^{\text{th}}$ and leads to an over-merging of tetrahedra if a small value of $\gamma^{\text{th}}$ is chosen. The criterion of Reboul et al. can overcome the latter drawback by imposing a merging level. However, it is not obvious to choose the level $L_1$ or $L_2$ or a further level. In addition, limiting artificially the pore size might lead to a sub-division of single pores into several smaller entities. In the next section, we introduce a new merging criterion that allows us to minimize the subjectivity in characterizing pores and constrictions without having to resort to an artificial limitation of pore sizes.

## 4 New merging criterion

### 4.1 Pore definition

The new criterion consists in merging hierarchically tetrahedra issued from the weighted Delaunay triangulation to form polyhedral sub-domains. Each sub-domain is composed of one or several neighboring tetrahedra. The concept of the inscribed void sphere defined for each tetrahedron is generalized to each polyhedral sub-domain. This is the largest void sphere that fits the best the void space within the sub-domain under consideration as illustrated in Figure 7.a. Given a sub-domain composed of $N$ solid particles, we define the following objective function whose variables are the center $\boldsymbol{X}$ and the radius $R$ of a void sphere:

$$f(\boldsymbol{X}, R) = \sum_{i=1}^{N} \mid d_i(\boldsymbol{X}, R) \mid, \tag{1}$$

where $d_i(\boldsymbol{X}, R)$ is the distance between the void sphere and a solid one $i$ with center $\boldsymbol{X}_i$ and radius $R_i$:

$$d_i(\boldsymbol{X}, R) = \|\boldsymbol{X} - \boldsymbol{X}_i\| - (R + R_i). \tag{2}$$

The objective function $f$ is minimized with respect to $\boldsymbol{X}$ and $R$ by using the Nelder-Mead simplex search algorithm implemented in the package Scipy. This minimization procedure takes the centers and the radii of the inscribed void spheres defined for all the tetrahedra comprised by the sub-domain as guess values of $\boldsymbol{X}$ and $R$. The resulting global minimizer defines then the center and the radius of the inscribed void sphere for the sub-domain. Physically, the inscribed void sphere can be thought of as the biggest base particle that can be included within the void space of the sub-domain and it touches at least four solid particles. It is worth mentioning that Al-Raoush et al. [2] proposed an optimization procedure based on the Nelder-Mead simplex search algorithm to identify the largest inscribed sphere that can fit within the void space formed

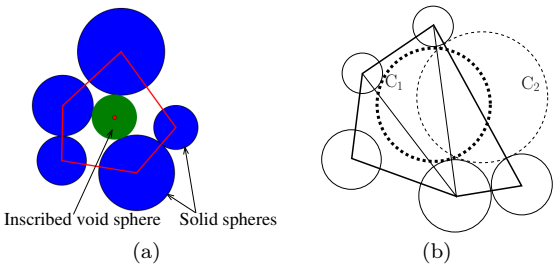


**Fig. 7** (a) 2D illustration of a sub-domain with the inscribed void sphere, and (b) the inscribed void sphere ($C_1$) of a sub-domain is not necessarily the biggest sphere ($C_2$) among the inscribed void spheres defined for each tetrahedron included by the sub-domain.

by a given tetrahedron and its adjacent ones. As the cost function was not presented in [2], the criterion used to identify this largest inscribed sphere is not known. Nevertheless, both procedures have the same property that they disassociate the resulting inscribed sphere from any particular tetrahedron. Instead of minimizing a cost function, Sufian et al. [31] proposed a combinatoric approach that consists in defining all possible configurations of four particles among all the involved particles. The inscribed sphere for each combination is determined and it is retained if it does not intersect other particles. The largest inscribed sphere is chosen among all retained ones. It should be noted that the combinatoric procedure of Sufian et al. is computationally less expensive than the minimization procedures proposed by Al-Raoush et al. and in the current criterion. In many cases, it gives the same inscribed sphere as the one obtained with the above minimization procedure. However, in some cases such as the case illustrated in Figure 7.b, the largest inscribed sphere obtained with the combinatoric procedure is not the one that fits the best the void space within the sub-domain in the sense of the minimum distance defined in (1).

We impose the three following conditions for each sub-domain so that the void space within it can define a single pore.

(i) The inscribed void sphere of a sub-domain must not intersect solid particles in its vicinity;
(ii) The center of the inscribed void sphere must be located inside the sub-domain for which it is defined;
(iii) The two inscribed void spheres of two adjacent sub-domains must be sufficiently separated from each other, *i.e.*, the overlap between them must be sufficiently small.

The 1st condition appears obvious. The 2nd one is a basic condition to obtain well-defined pore geometries. By enforcing this condition, all the flat tetrahedra issued from Delaunay triangulation are identified and then merged to its neighbors. The 3rd condition needs a criterion to assess separation between two adjacent inscribed void spheres. We use a criterion similar to the one used by Shire and O'Sullivan [27] for inscribed void spheres defined for tetrahedra (see Section 3). The inscribed void spheres defined for two adjacent sub-domains

are sufficiently separated if their relative overlap $\gamma = \delta / \min(d_i, d_j)$ ($\delta$ is the overlap; and $d_i$ and $d_j$ are their diameters) is smaller than a user-specified value $\gamma^{\text{th}}$.

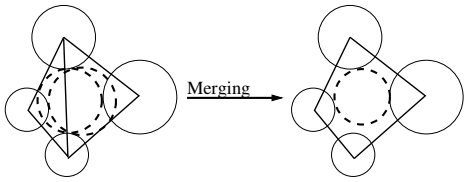


**Fig. 8** Merge two adjacent sub-domains if the inscribed void sphere of a sub-domain intersects solid spheres of the other sub-domain.

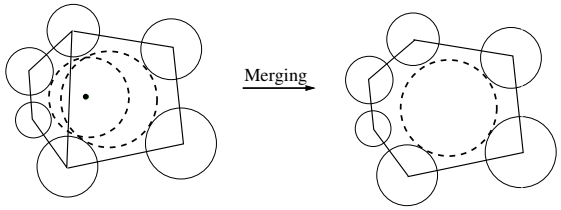


**Fig. 9** Merge two adjacent sub-domains if the center of an inscribed void sphere is located outside the corresponding sub-domain but inside the other sub-domain.

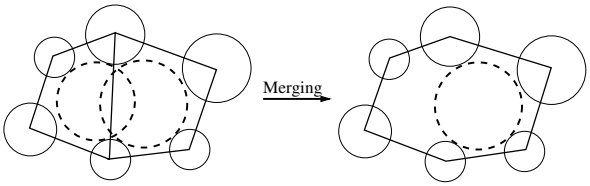


**Fig. 10** Merge two adjacent sub-domains if the relative overlap $\gamma$ between their inscribed void spheres is greater than the user-specified value $\gamma^{\text{th}}$.

The granular assembly is first subdivided into tetrahedra. Each tetrahedron with its associated inscribed void sphere is initially considered as a sub-domain. Every couple of adjacent sub-domains are subsequently merged if they do not fulfill one of the three conditions mentioned above. It is important to note that

*merging two adjacent sub-domains results in a new sub-domain for which a new inscribed void sphere is identified.* Firstly, if the inscribed void sphere of a sub-domain intersects some solid particles of the other sub-domain, these two sub-domains are merged together to form a new sub-domain as illustrated in Figure 8. Next, any couple of sub-domains are merged if the center of an inscribed void sphere is located outside the corresponding sub-domain but inside the other sub-domain (Figure 9). Finally, if the relative overlap $\gamma$ between two inscribed void spheres is greater than the user-specified admissible overlap $\gamma^{\text{th}}$, the two corresponding sub-domains are merged as illustrated in Figure 10.

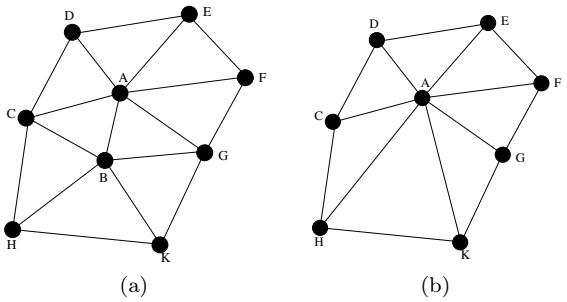


**Fig. 11** Graph (a) before and (b) after merging the vertex B to the vertex A.

For the merging procedure, the sub-domains are represented by a graph where each vertex is a sub-domain, and each edge joins a couple of adjacent sub-domains. This graph is updated whenever a couple of sub-domains is merged. As illustrated in Figure 11, when the vertex B is merged to the vertex A, the first one and the edge between them is deleted, and all the edges between the vertex B and its neighbors are moved to the vertex A.

Figure 12.a presents the procedure for the whole merging process where the three conditions mentioned above are sequentially enforced against all couples of adjacent sub-domains. The iterative sub-procedure to enforce each condition is shown in Figure 12.b. At each iteration of this sub-procedure, a couple of adjacent sub-domains that do not fulfill the condition under consideration are merged; subsequently, a new inscribed void sphere is identified for the resulting new sub-domain. The couples of adjacent sub-domains are handled in descending order of the intersection between void and solid spheres (normalized by the void sphere diameter) for the 1st condition and of the relative overlap $\gamma$ between two void spheres for the 3rd condition. On the other hand, the couple of adjacent sub-domains are randomly chosen at each iteration for the 2nd condition. It is worth mentioning that the distance between a sub-domain and the center of its inscribed void sphere, normalized by the radius of the latter, can be computed and the sub-domains can be handled in the descending order of this distance for the 2nd condition. Nevertheless, the results obtained with both manners of handling sub-domains are almost

the same. As computing the distance from a point to a polyhedral sub-domain is quite costly, the random handling of sub-domains for the 2nd condition is adopted in the proposed merging criterion. The merging steps according to the 1st and 2nd conditions are called *primary merging procedure* (abbreviated as PM procedure), for which no user-defined value is needed. It is important to highlight that whenever a couple of adjacent sub-domains are merged by the new criterion, a new inscribed sphere is identified for the resulting sub-domain. This key feature in addition to the primary merging procedure allow us to reduce significantly the sensitivity of the resulting pore network to the user-specified value $\gamma^{\text{th}}$ as shown in the following. However, they make the computation about 1.6 more costly in comparison with existing criteria. It is worth mentioning that in the current version of our Python code, the package igraph [5] is used to link neighboring pores when implementing the new and existing criteria. Around 50% of the total computation time is used to update the pore network whenever two neighboring pores are merged together for all criteria. Searching and updating inscribed void spheres consume less than 10% of the total computation time. Further efforts will be made to optimize the code and reduce the computation time for updating the pore network.

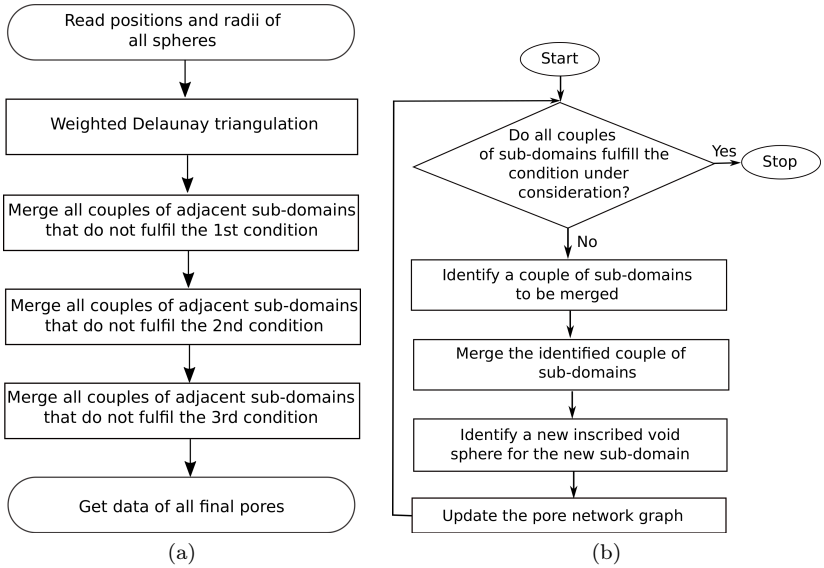


**Fig. 12** (a) Procedure for the whole merging process and (b) sub-procedure to enforce a given condition against all couples of adjacent sub-domains.

Figure 13 shows PSDs obtained for the UGL sample by using the new merging criterion presented above. One can remark that the primary merging procedure (PM curve) leads to a great change of the PSD compared to that issued directly from Delaunay triangulation ($L_0$ curve). In fact, the flat tetra-

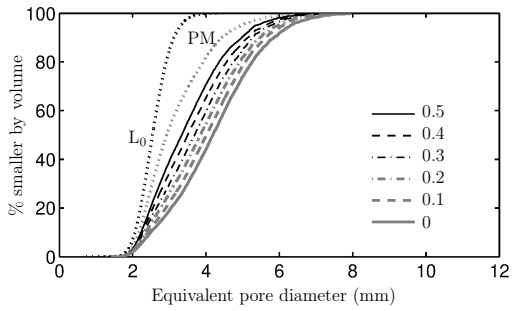


**Fig. 13** PSDs obtained for the UGL sample by using the new merging criterion with the threshold value $\gamma^{\text{th}}$ varied between 0.5 and 0. PM stands for the primary merging procedure.

hedra that do not fulfill the above 1st and 2nd conditions occupy about 36% by number of the tetrahedra resulting from the Delaunay triangulation. It is worth noting that all the tetrahedra near the boundaries are excluded from the analysis. The percentage of flat tetrahedra is actually higher (45%) for the tetrahedra near the boundaries. The PM procedure allows these flat tetrahedra to be merged to their neighbors, giving rise to bigger sub-domains, each of which is a potential candidate for a single pore. However, there is still an important portion of sub-domains whose inscribed void spheres overlap greatly those of their neighbors. Therefore, these sub-domains continue to be merged by imposing the 3rd condition with a user-specified value $\gamma^{\text{th}}$. It can be seen that the PSD changes as $\gamma^{\text{th}}$ is decreased. However, by comparing Figures 13 and 4, we can see that the PSD obtained with the new merging criterion is much less sensitive to the user-specified value $\gamma^{\text{th}}$ than that obtained with the criterion of Shire and O'Sullivan. As shown in Figure 14, by decreasing $\gamma^{\text{th}}$ from 1 to 0, the equivalent pore diameters $D^*_{50}$ and $D^*_{75}$, which correspond to 50% and 75% by pore volume, increase actually by a factor of 2.4 for the criterion of Shire and O'Sullivan, compared to a factor of 1.4 for the new merging criterion. It should be noted that $\gamma^{\text{th}} = 1$ for the former criterion corresponds to the level $L_0$ issued from Delaunay triangulation, while this value for the latter criterion corresponds to the configuration given by the PM procedure.

It is interesting to note in Figure 13 that the new merging criterion does not result in a significant increase in the maximum pore size as $\gamma^{\text{th}}$ is decreased, even with $\gamma^{\text{th}} = 0$ (no overlap between inscribed void spheres is allowed). This means that the new criterion does not over-merge tetrahedra, a drawback of the criterion of Shire and O'Sullivan as discussed in Section 3. This is attributed to the fact that whenever a couple of adjacent sub-domains are merged at each iteration, a new inscribed void sphere is identified for the resulting new sub-domain. By doing so, the inscribed void sphere is more and more enclosed by the solid spheres of the new sub-domain, leading to a progressive reduction of the overlap with its neighbors.

Pores have been defined in this section by the proposed new merging criterion including three conditions required for each couple of adjacent sub-

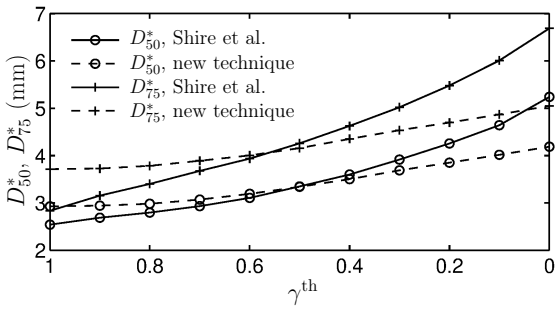


**Fig. 14** Equivalent pore diameters $D^*_{50}$ and $D^*_{75}$ for the UGL sample versus the user-specified value $\gamma^{\text{th}}$ obtained with the criterion of Shire and O'Sullivan and the new merging criterion.

domains. In the next section, the size of each constriction shared by two adjacent pores is defined.

### 4.2 Constriction definition

For methods based on Delaunay triangulation, the void space on each triangular face joining three neighboring particle centers can be considered as a constriction between the two adjacent pores that share this triangular face [22,27,34]. Reboul et al. [22] defined the size of each constriction as the diameter of the largest empty disk that can fit within the void space on the triangular face under consideration as illustrated in Figure 5.b. If this largest empty disk intersects some solid spheres in the vicinity, a new largest empty disk is identified by taking into consideration the solid disks resulting from intersections between these solid spheres and the plane defined by the triangular face. It should be noted that as the largest empty disk is only defined on the plane of the triangular face, an empty sphere with the same center and diameter as those of the largest empty disk may intersect solid particles out of the plane as illustrated in Figure 15. This means that a particle with the same diameter may not pass through the constriction, hence the constriction size is over-estimated.

Instead of considering the largest empty disk on each triangular face to define the constriction size, we consider a *largest empty sphere* for the set of all triangular faces shared by two adjacent pores. This is the largest sphere that can pass through the void space between the set of the common solid particles as illustrated in Figure 16. This largest empty sphere is identified by minimizing the cost function defined in Equation (1) where all the solid particles that form the constriction are taken into consideration. The difference in comparison with the minimization procedure described in Section 4.1 when identifying the inscribed void sphere for a sub-domain is that the center of the candidate empty sphere is enforced to lie in one of the planes defined by the common triangular faces. The centers and radii of the largest empty disks

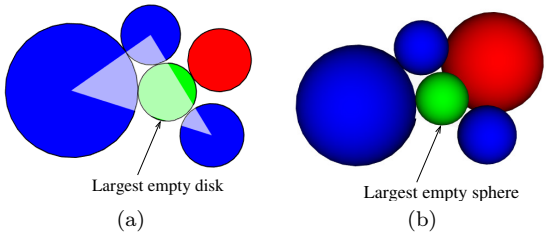


**Fig. 15** An empty sphere with the same center and diameter as those of the largest empty disk (a) might intersect adjacent solid spheres out of the plane (b).

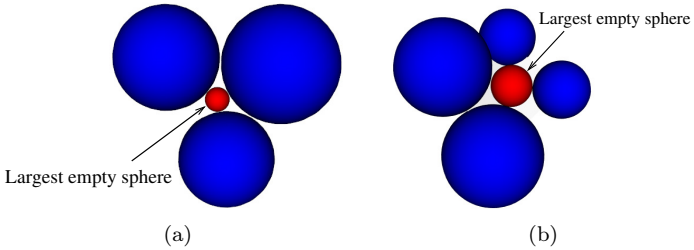


**Fig. 16** A constriction can be formed by one triangular face (a) or several adjacent triangular faces (b).

defined on each triangular face are considered as guess values and the global minimizer gives the largest empty sphere. For most constrictions except those near the boundaries, the identified largest empty sphere does not intersect solid spheres in close proximity. In the opposite case, the intersected solid spheres are included in the cost function (1) to identify a new largest empty sphere. It should be noted that this modified definition of constrictions implies a merging of all the triangular faces shared by two adjacent pores to form only one constriction; however, these common triangular faces are not required to be coplanar as shown in Figure 16.b. In addition, the largest empty disk defined by Reboul et al. and the largest empty sphere defined above give the same size for the constrictions formed by only one triangular face of three particles. If a constriction is formed by several triangular faces, its size is defined not only by the void area on each face but also by the void space in close proximity. This is the main difference in comparison with the definition proposed by Reboul et al. [22].

Figure 17 shows the CSD given by largest empty spheres for the UGL sample, compared to that given by largest empty disks. The new merging criterion presented in the previous section with the admissible overlap $\gamma^{\text{th}} = 0$ is used to define the pores. It is clear that the constriction size is overestimated by the largest empty disk. However, this overestimation is small because a

majority of constrictions (about 88%) are formed by only one triangular face. This is also true for the other samples.

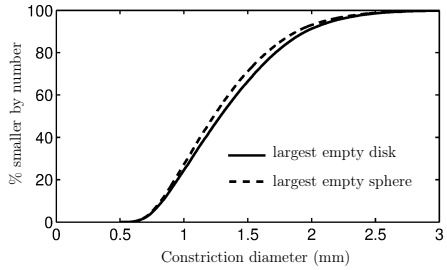


**Fig. 17** Comparison between the CSD given by largest empty disks and the CSD given by largest empty spheres for the UGL sample where the pores are defined by the new merging criterion with $\gamma^{\text{th}} = 0$.

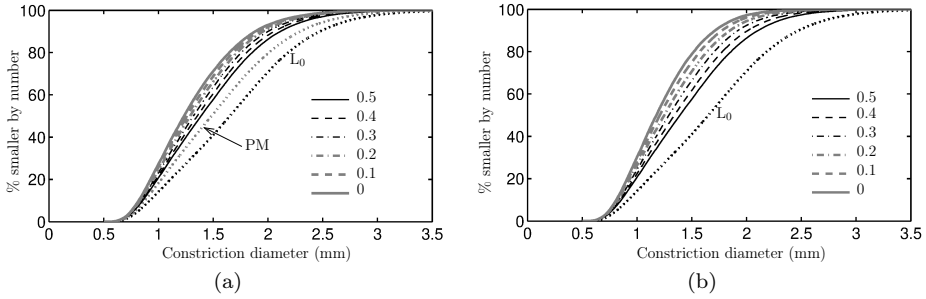


**Fig. 18** (a) CSDs obtained for the sample UGL with various user-specified values $\gamma^{\text{th}}$ by using the new merging criterion, compared with those (b) obtained with the criterion of Shire and O'Sullivan

The definition of constrictions is closely related to the way where the pores are defined. As the pore characteristics obtained with the new merging criterion depend on the user-specified admissible overlap $\gamma^{\text{th}}$, so do the constriction characteristics. This can be seen in Figure 18.a where the CSD curve is shifted to the left as $\gamma^{\text{th}}$ is decreased. However, like the PSD, the CSD obtained with the new merging criterion is less dependent on $\gamma^{\text{th}}$ than that given by the criterion of Shire and O'Sullivan shown in Figure 18.b. The latter varies largely from the curve $L_0$ to the curve of $\gamma^{\text{th}} = 0$ as $\gamma^{\text{th}}$ is varied from 1 to 0. Shire and O'Sullivan [27] also observed a strong dependence of the CSD obtained with their criterion on the user-specified value $\gamma^{\text{th}}$.

As shown in Figure 19, the constriction diameters $D_{c50}$ and $D_{c75}$, which correspond to 50% and 75% by number of constrictions, are reduced by a factor of about 1.4 when $\gamma^{\text{th}}$ is decreased from 1 to 0 for the criterion of Shire and

O'Sullivan. The new merging criterion associated with the primary merging procedure described in Section 4.1 allows us to reduce significantly the range of variation of the CSD. Indeed, as $\gamma^{\text{th}}$ is decreased from 1 to 0, the constriction diameters $D_{c50}$ and $D_{c75}$ are reduced by a factor of about 1.2. It is worth mentioning that the CSDs given by both criteria are much less sensitive to $\gamma^{\text{th}}$ than the PSDs (see Figures 4 and 13).

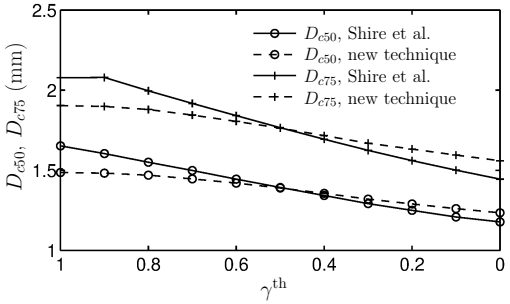


**Fig. 19** Constriction diameters $D_{c50}$ and $D_{c75}$ versus the user-specified value $\gamma^{\text{th}}$ for the criterion of Shire and O'Sullivan and the new merging criterion.

Although the new merging criterion allows us to reduce greatly the dependence of the pore and constriction characteristics upon the user-specified value $\gamma^{\text{th}}$, the choice of this threshold value remains crucial and is subjected to the subjectivity of the user. Figure 20 illustrates three cases (a), (b) and (c) where the inscribed void spheres of two adjacent pores strongly overlap, slightly overlap and do not overlap, respectively. It would be acceptable to consider that the two pores in case (a) need to be merged together to form a single pore, while those in case (c) can be considered as separated pores. On the other hand, the subjectivity lies in case (b) where it is not easy to decide whether the two adjacent pores are separated or belong to a single entity. A strict pore separation criterion implies that $\gamma^{\text{th}} = 0$, *i.e.*, two pores are fully separated if their inscribed void spheres do not overlap each other. This threshold value is adopted in the following for the new merging criterion and for the criterion of Shire and O'Sullivan.

## 5 Comparison of different merging criteria

In this section, we compare the PSD and CSD given by the new merging criterion to those obtained with the criterion of Shire and O'Sullivan and with the $L_1$ and $L_2$ criteria of Reboul et al. The uniformly graded (UG), gap-graded (GG) and widely graded (WG) samples at loose and dense states presented in Section 2 are considered for the comparison.

Figure 21 shows the PSDs and CSDs obtained for the UGL and UGD samples by using the four different merging criteria mentioned above. It can

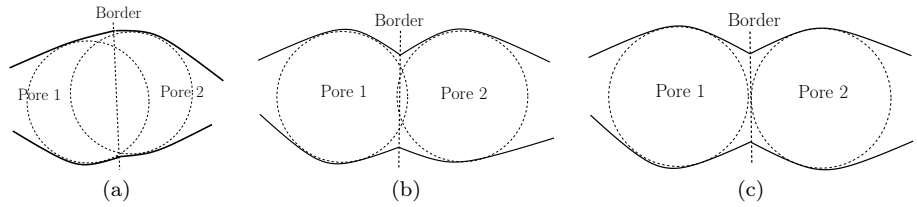


**Fig. 20** Illustration of two adjacent pores whose inscribed void spheres (a) strongly overlap, (b) slightly overlap and (c) do not overlap. Solid curves represent the pore walls, while dashed circles represent inscribed void spheres.

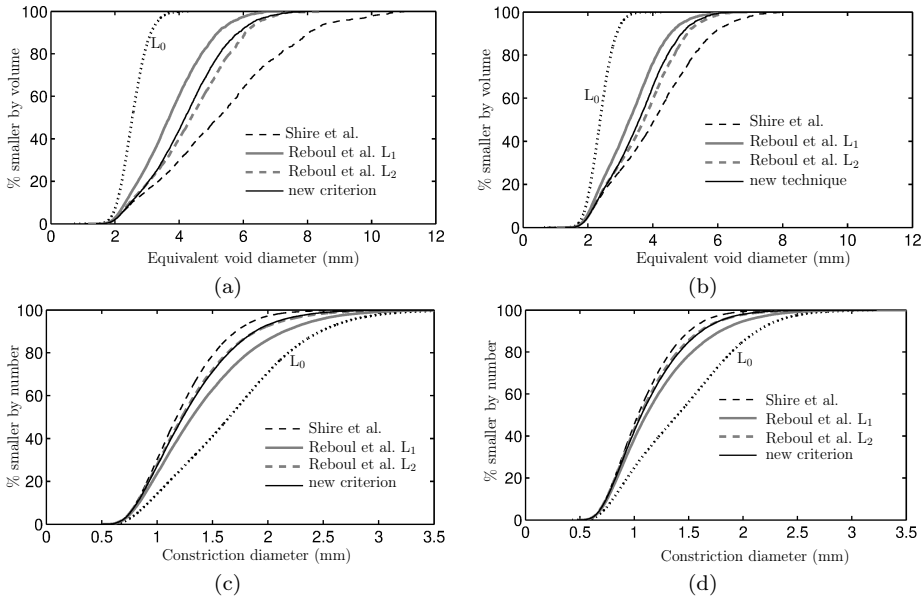


**Fig. 21** (a-b) PSDs and (c-d) CSDs given by the four merging criteria for the UGL (left column) and UGD (right column) samples.

be seen in Figures 21.a and 21.b that the PSD given by the criterion of Shire and O'Sullivan is the rightmost one and very different from those given by the other criteria, owning to its excessive merging of tetrahedra. Indeed, as shown in Figure 22 for the UGL sample, the numbers of tetrahedra included in each pore obtained with this criterion vary largely up to 97 and are not fully represented in the chosen scale on the abscissa (the pores with more than 20 tetrahedra represent 20% of the void volume of the sample). On the other hand, the $L_1$ criterion results in the leftmost PSD. It is interesting to note that the new criterion gives a PSD intermediate between those given by the $L_1$ and $L_2$ criteria; moreover, it is closer to the curve of $L_2$ than that of $L_1$. More specifically, the PSDs given by the new and $L_2$ criteria are close for pores of small sizes but differ for pores of medium and big sizes. This result means

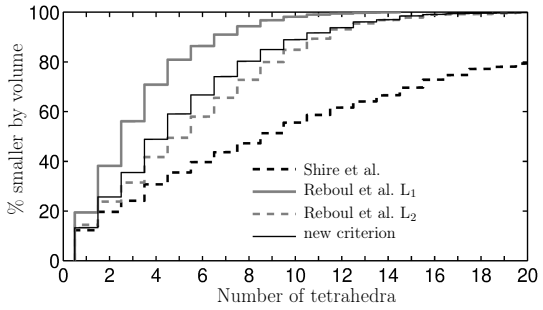


**Fig. 22** Distributions of numbers of tetrahedra included in each pore given by the four merging criteria for the UGL sample. Each stairstep graph represents the cumulative percentage by volume of all the pores whose numbers of tetrahedra are smaller than or equal to a given value on the abscissa.

that merging of neighboring tetrahedra according to the new criterion does not go beyond the level $L_2$ (see Figure 5). It is worth mentioning that the $L_2$ criterion presents advantages but also disadvantages in comparison with the $L_1$ criterion. Indeed, the $L_2$ criterion allows the merging process to be extended to the tetrahedra of level $L_2$ in some cases, allowing pores to be fully enclosed by solid particles (for example, the case illustrated in Figure 6.b). However, it gives rise to complex clusters, each of which is composed of a central tetrahedron and all its neighbors of levels $L_1$ and $L_2$. The new merging criterion takes advantage of the $L_2$ criterion to define pores of small sizes but remediates the drawback of the latter when defining pores of medium and big sizes by merging selectively but not all tetrahedra of level $L_2$. Figure 22 shows clearly that the new criterion merges more tetrahedra than the $L_1$ criterion but fewer than the $L_2$ criterion to define pores of medium and big sizes. It is worth noting that by merging at most adjacent tetrahedra, which is the case for the criterion of Shire and O'Sullivan with $\gamma^{\text{th}} = 0$, 55% by number of the pores are formed by single tetrahedra but they occupy only 12% of the total void volume of the sample. The new and $L_2$ criteria give almost the same value, while the $L_1$ criterion gives a higher value of about 19% by volume. This can be attributed to the fact that by limiting the merging process to the level $L_1$, some tetrahedra of level $L_2$ are not merged to its neighbors as illustrated in Figure 6.b.

As shown in Figures 21.c and 21.d, as a consequence of its excessive merging of tetrahedra, the criterion of Shire and O'Sullivan results in more constrictions of smaller sizes in comparison with the CSD given by the new criterion, and then the leftmost CSD. On the other hand, the criterion $L_1$ results in more constrictions of bigger sizes, and then the rightmost CSD. As for the $L_2$ criterion, it gives a CSD curve very close to that of the new criterion. One can also remark that the difference between the CSDs is much less noticeable than the difference between the PSDs observed in Figures 21.a and 21.b. In

addition, the PSDs and CSDs given by the four merging criteria get closer for the UGD sample in comparison with those obtained for the UGL sample.

When 20% of fine content is added to the above UGL sample, the latter becomes the GGL sample. The fine particles fill the voids between the coarse particles, reducing greatly pore sizes and constriction sizes in this sample. Figure 23 presents the PSDs and CSDs for the GGL sample. It can be seen that, on the whole, the different merging criteria give quite close PSD and CSD curves except the PSD given by the criterion of Shire and O'Sullivan. A small difference between the CSD given by the $L_1$ criterion and the others can be also observed.

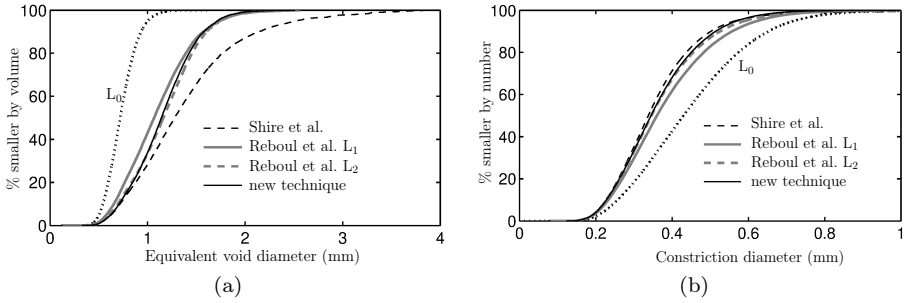


**Fig. 23** (a) PSDs and (b) CSDs given by the four merging criteria for the GGL sample.

To give a further comparison between the PSDs and CSDs given by the four different merging criteria for all the six simulated samples presented in Table 1, we present the equivalent pore diameters $D^*_{50}$ and $D^*_{75}$ in Table 2 and the constriction diameters $D_{c50}$ and $D_{c75}$ in Table 3 for each sample. For each parameter, the value given by the new criterion is considered as the reference value $x^{\text{ref}}$, and a value $x$ given by another criterion is compared to the reference one by calculating the relative difference $(x - x^{\text{ref}})/x^{\text{ref}}$. It can be seen that the criterion of Shire and O'Sullivan gives quite bigger pore sizes for all the samples, while the $L_1$ criterion results in smaller pore sizes in comparison with those given by the new criterion. For the dense samples GGD and WGD, $D^*_{50}$ and $D^*_{75}$ given by these two criteria get closer to those given by the new criterion with relative differences in $D^*_{50}$ and $D^*_{75}$ smaller than 8%. On the other hand, the $L_2$ and the new criterion give quite close PSDs with relative differences in $D^*_{50}$ and $D^*_{75}$ smaller than 6% for all the samples.

In comparison to the divergence between the PSDs resulting from the four merging criteria, the divergence between the resulting CSDs is much less noticeable. As shown in Table 3, relative differences in $D_{c50}$ and $D_{c75}$ are actually smaller than 8% for the criterion of Shire and O'Sullivan and 10% for the $L_1$ criterion. In addition, they tend to converge for the gap-graded and widely graded samples, in particular for the dense ones GGD and WGD. For these samples, the criterion of Shire and O'Sullivan gives actually almost the same

CSDs as those given by the new criterion, while there is still a small difference of about 6% for the $L_1$ criterion. It should be noted that the $L_2$ and the new criterion give very close CSDs for all the samples.

**Table 2** Equivalent pore diameters $D^*_{50}$ and $D^*_{75}$ given by the new criterion and relative differences in $D^*_{50}$ and $D^*_{75}$ given by the other criteria for different samples.

| Sample | New criterion | | Shire et al. | | Reboul et al. $L_1$ | | Reboul et al. $L_2$ | |
|---|---|---|---|---|---|---|---|---|
| | $D^*_{50}$(mm) | $D^*_{75}$(mm) | $D^*_{50}$ | $D^*_{75}$ | $D^*_{50}$ | $D^*_{75}$ | $D^*_{50}$ | $D^*_{75}$ |
| UGL | 4.19 | 5.05 | +25% | +32% | -12% | -11% | +5% | +6% |
| UGD | 3.58 | 4.28 | +13% | +18% | -8% | -8% | +4% | +4% |
| GGL | 1.14 | 1.37 | +11% | +21% | -6% | -3% | +2% | +2% |
| GGD | 1.00 | 1.17 | +4% | +8% | -4% | 0% | +1% | +3% |
| WGL | 1.03 | 1.24 | +11% | +18% | -9% | -8% | +2% | +2% |
| WGD | 0.91 | 1.09 | +4% | +6% | -5% | -6% | +1% | +2% |

**Table 3** Constriction diameters $D_{c50}$ and $D_{c75}$ given by the new criterion and relative differences in $D_{c50}$ and $D_{c75}$ given by the other criteria for different samples.

| Sample | new criterion | | Shire et al. | | Reboul et al. $L_1$ | | Reboul et al. $L_2$ | |
|---|---|---|---|---|---|---|---|---|
| | $D_{c50}$(mm) | $D_{c75}$(mm) | $D_{c50}$ | $D_{c75}$ | $D_{c50}$ | $D_{c75}$ | $D_{c50}$ | $D_{c75}$ |
| UGL | 1.23 | 1.56 | -4% | -8% | +7% | +10% | +1% | +1% |
| UGD | 1.07 | 1.34 | -4% | -5% | +4% | +7% | +1% | +1% |
| GGL | 0.35 | 0.43 | -3% | -2% | +3% | +7% | 0% | 0% |
| GGD | 0.29 | 0.36 | 0% | 0% | +3% | +6% | 0% | 0% |
| WGL | 0.31 | 0.38 | -3% | -3% | +3% | +8% | 0% | +3% |
| WGD | 0.26 | 0.33 | 0% | -3% | +4% | +6% | 0% | 0% |

Figure 24 shows a comparison of the CSDs given the four considered merging criteria for the UGL and GGL samples by plotting the probability density function (PDF) versus the constriction diameter. It is interesting to note that that the four different merging criteria result in nearly the same CSD mode (the constriction diameter corresponds to the maximum of the PDF) for both samples (this is also true for the other samples). However, the maximum PDFs of constriction sizes are significantly different. In comparison with the CSDs given by the new and the $L_2$ criterion, the criterion of Shire and O'Sullivan gives narrower CSDs, while the $L_1$ criterion results in wider CSDs.

## 6 Controlling constriction size $D^*_c$ estimated with the CSD

To the best of our knowledge, there is not a unique solution for the CSD of a granular material since pores and constrictions are geometrically too complex to be precisely defined. As a consequence, the CSD given by a method cannot be directly confronted against experimental data. However, one can indirectly validate a CSD, for instance, by using it to estimate the controlling constriction size $D^*_c$ of a granular material, which is the largest diameter of base particles

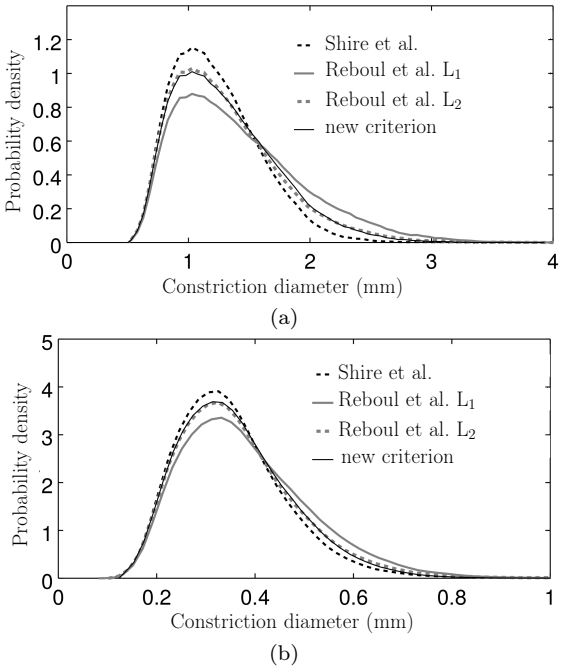


**Fig. 24** Probability density function versus constriction diameter obtained with the four merging criteria for (a) UGL and (b) GGL.

that can pass through the void space within the material, and comparing this value to that obtained experimentally. Shire and O'Sullivan [28] incorporated CSDs extracted from virtual granular filters into a pore network model based on a random walk algorithm to assess their retention efficiency. The authors found that the controlling constriction size $D_c^*$ given by the model is, on the whole, in good agreement with experimental data.

Seblany [24] simulated dry filtration tests (base particles move inside the pore space of the filter under gravity) and hydraulic ones by using the DEM coupled to a fluid model to determine values of $D_c^*$ of virtual filters composed of spherical particles. Interestingly, it was found that this controlling constriction size $D_c^*$ is closely related to the modal diameter of the CSD. As a result, the author proposed to take the controlling constriction size $D_c^*$ of a granular material as the modal value of its CSD. This approach is adopted here to determine controlling constriction sizes $D_c^*$ of the six samples considered in our study. It is worth mentioning that a granular material can be used as a filter if it is internally stable and effective to retain base particles according to empirical retention criteria that can be written in the form $D_c^* < d_I$, i.e. the controlling constriction size $D_c^*$ of the filter must be smaller than an indicative size $d_I$ chosen for base soils [14]. The $d_I$ value is often taken as the diameter $d_{85}$ of the base soil [26]. The controlling constriction size $D_c^*$ of a filter is then

the key parameter to assess its retention effectiveness against a given base soil. As shown in Section 2, the three GSDs considered in the current study are stable; therefore they can be used to design filters if they satisfy retention criteria. In comparison with uniformly graded materials (UG), widely graded or gap-graded materials (GG and WG) might be more susceptible to internal erosion; however, sizes of pores and constrictions in these materials are greatly smaller than those of uniformly graded materials (see Tables 2 and 3) so they can be used to design filters against fine soils such as silts and clays. Indeed, Sherard et al. [26] showed that sand and gravel mixtures that are not strongly gap-graded are good filters for fine silts and clays.

Table 4 shows the controlling constriction sizes $D_c^*$ estimated from the CSDs obtained with the new merging criterion for the six samples. It is shown that the values of $D_c^*$ for the GG and WG samples are significantly smaller than those of the UG samples. In addition, $D_c^*$ for each gradation gets smaller when the material gets denser. Kenney and Lau [11] proposed the following empirical rule $D_c^* < 0.2D_{15}$ to estimate the controlling constriction size $D_c^*$ for dense stable filters with relative densities from 70% to 100%. It can be seen that the values of $D_c^*$ estimated from the CSDs for the dense samples UGD and WGD are in good agreement with the above empirical rule ($D_c^*/D_{15} = 0.21$ for the UGD is slightly higher than the empirical value of 0.2). For the dense sample GGD, the ratio $D_c^*/D_{15} = 0.27$ is significantly higher than the empirical value of 0.2. Seblany [24] also found in the author's numerical filtration tests that values of $D_c^*$ for gap-graded samples are higher than those given by Kenney and Lau's empirical rule. It is worth mentioning that this empirical rule has been established based on experimental tests on well graded soils. Its validity for gap-graded materials is not well studied yet.

**Table 4** Controlling constriction sizes $D_c^*$ estimated by using CSDs in comparison with the particle diameters $D_{15}$ for different samples.

| Sample | $D_c^*$ (mm) | $D_{15}$ (mm) | $D_c^*/D_{15}$ |
|---|---|---|---|
| UGL | 1.03 | 4.12 | 0.25 |
| UGD | 0.86 | 4.12 | 0.21 |
| GGL | 0.31 | 1.07 | 0.29 |
| GGD | 0.29 | 1.07 | 0.27 |
| WGL | 0.27 | 1.36 | 0.2 |
| WGD | 0.22 | 1.36 | 0.16 |

As stated by Kenney and Lau [12], a granular material contains loose particles that are located within the pores of the primary fabric. These loose particles support no or very little stresses so they can be detached and transported by water flow. If the sizes of constrictions of the primary fabric are large enough, a fraction of the loose particles are washed out from the material. This phenomenon is called *internal erosion*. Like physical materials, the numerical samples considered in this study contain loose particles. As mentioned in Section 2, the sample generation without gravity used in the current study results in the *rattlers* that are floating within pores. Although this sample generation

is artificial, the rattlers are not completely unphysical. They correspond actually to physical particles that are almost free within pores and carry no or very little stresses. For instance, this is the case for gap-graded materials with low fine content (the samples GGL and GGD in our study). These rattlers and other particles that carry little stresses might be detached by the water flow; however, the rattlers are the most likely to be detached as they carry no stresses. It should be noted that although the six samples considered here are stable according to empirical rules, it does not mean that all of their particles are not susceptible to internal erosion. It is actually difficult to define a distinct boundary between internal stability and instability as internal erosion is a complex phenomenon that depends not only on the material properties but also on stress conditions and hydraulic conditions. Rather than making a clear distinction between stable and unstable soils, Marot et al. [19] proposed to classify soils from strongly erodible to strongly resistant to internal erosion.

Particles that do not take part in the primary fabric of the material and are susceptible to be eroded should be discarded to obtain an accurate description of its pore space. However, identification of these unstable particles is very challenging as it requires to take into account not only their stress state but also hydraulic conditions and characteristics of the pore network of the solid skeleton. No accurate method has been established so far. In the absence of such a method, let us now assume an unfavorable situation that all the rattlers are eroded from the samples and study how their CSDs change. Table 5 presents porosities $n$ and coefficients of uniformity $C_u$ of the six samples before and after removing the rattlers. It can be seen that the loose samples contain such big numbers of rattlers that removing them leads to a great increase in their porosity and a decrease in their coefficient of uniformity, particularly for the samples GGL and WGL. Most of the fine particles are removed from the sample GGL, while the GSD for the sample WGL without rattlers, which is initially widely graded, becomes narrowly graded. We can also remark that a great fraction of rattlers at the loose state become active at the dense state. As a consequence, removing the rattlers from the dense samples does not cause a great change to these samples except the sample GGD where the fine content is reduced from 20% to 10% as shown in Figure 25.

**Table 5** Porosities $n$ and coefficients of uniformity $C_u$ of the six samples before and after removing the rattlers.

| | Before | | After | |
|---|---|---|---|---|
| Sample | $n$ | $C_u$ | $n$ | $C_u$ |
| UGL | 0.41 | 1.7 | 0.51 | 1.6 |
| UGD | 0.36 | 1.7 | 0.39 | 1.6 |
| GGL | 0.31 | 3.7 | 0.47 | 1.4 |
| GGD | 0.26 | 3.7 | 0.35 | 1.4 |
| WGL | 0.23 | 10.4 | 0.48 | 2.6 |
| WGD | 0.19 | 10.4 | 0.22 | 8.7 |

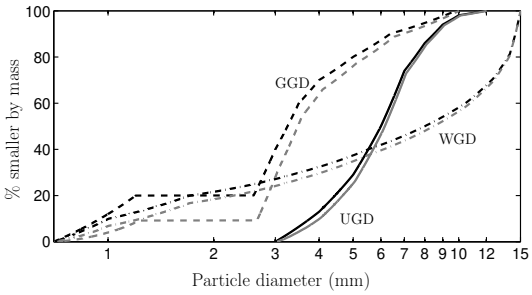


**Fig. 25** GSDs of the samples UGD, GGD and WGD when all the rattlers are removed (gray curves) in comparison with those with rattlers (black curves).

The CSDs of the three dense samples UGD, GGD and WGD without rattlers are compared to those with rattlers in Figure 26. It can be seen that the CSDs for the samples UGD and WGD change slightly but their modal values remain unchanged. Regarding the sample GGD, its CSD without rattlers changes greatly and becomes bimodal in comparison with the unimodal distribution for the case with the rattlers. It was shown in [24] that the controlling constriction size $D_c^*$ is close to the largest mode for a bimodal CSD. On can remark in Figure 26.b that the largest mode of the bimodal CSD is almost the same as the one of the unimodal CSD so the estimated value of $D_c^*$ for the sample GGD does not change. As shown in Table 6, the ratio $D_c^*/D_{15}$ for the sample GGD is greatly reduced from 0.27 for the case with rattlers to 0.11 for the case without rattlers, which is significantly smaller than the empirical upper limit of 0.2 mentioned above. This result points out that empirical rules linking the controlling constriction size $D_c^*$ to the particle diameter $D_{15}$ should be used with caution for gap-graded soils with low fine content. For such soils, the voids between the coarse particles are underfilled by fine particles; hence, a significant fraction of the fine particles do not take part in the primary fabric. As a result, the particle diameter $D_{15}$ of the primary fabric is bigger than $D_{15}$ of the whole gradation curve.

**Table 6** Controlling constriction size $D_c^*$ estimated by using the CSD in comparison with the particle diameter $D_{15}$ for the dense samples without rattlers.

| Sample | $D_c^*$ (mm) | $D_{15}$ (mm) | $D_c^*/D_{15}$ |
|---|---|---|---|
| UGD | 0.91 | 4.35 | 0.21 |
| GGD | 0.3 | 2.76 | 0.11 |
| WGD | 0.22 | 1.59 | 0.14 |

Although the internal state of an eroded soil cannot be relevantly represented by simply removing all the rattlers, the above study shows an interesting result that the CSDs of the considered dense samples are actually affected by the presence of the rattlers; nevertheless, their modal values, which were

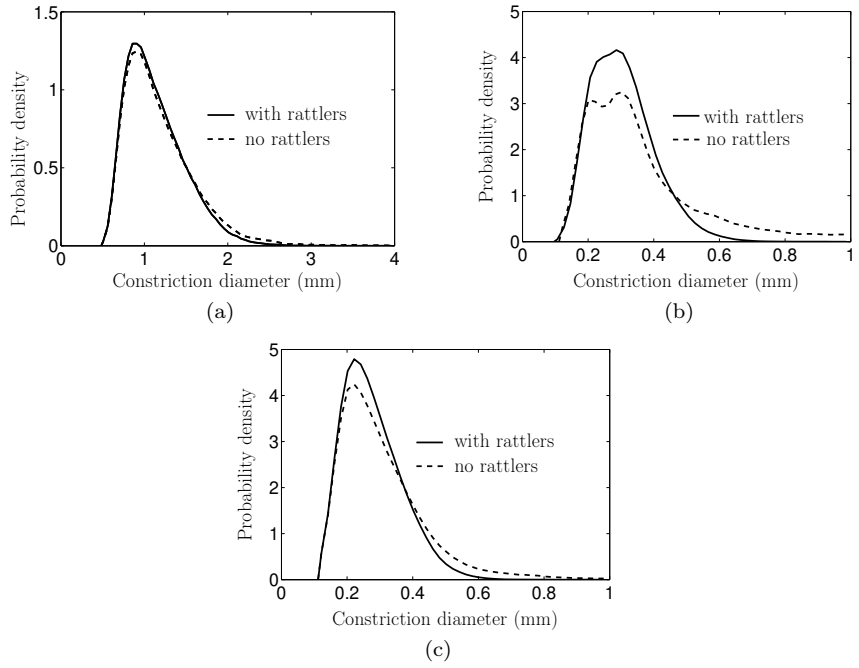


**Fig. 26** Probability density function versus constriction diameter given by the new merging criterion for (a) UGD, (b) GGD and (c) WGD with and without rattlers.

taken as the controlling constriction sizes $D_c^*$, remain unchanged when all the rattlers are removed. This result reveals that the controlling constriction size $D_c^*$ of a granular material might be an own characteristic of its primary fabric rather than a characteristic of the whole material. Further studies should be carried out to confirm this result by using a sample generation procedure that allows us to eliminate unstable particles. For instance, when the compaction finishes, a driving force similar to the seepage force can be applied to particles so that unstable particles can be moved, dislodged or leave the sample.

## 7 Conclusions

Determining pore sizes and constriction sizes within a granular material is vital to assess its ability to retain finer particles transported by seepage flow within its void space. In this paper, we determined these characteristics from virtual granular samples of spherical particles simulated with the DEM. A new criterion was developed to merge tetrahedra issued from the weighted Delaunay triangulation to form single pores. The concept of inscribed void sphere defined for each tetrahedron is extended to a polyhedral sub-domain (a cluster of tetrahedra). This inscribed void sphere fits the best the void space within

the sub-domain and is identified by a minimization procedure. Flat tetrahedra are efficiently removed by a primary merging procedure that enforces two basic geometric conditions for each sub-domain. Subsequently, couples of adjacent sub-domains are merged depending on the level of overlap between their inscribed void spheres. Each time a couple of sub-domains is merged, a new inscribed void sphere is identified for the resulting new sub-domain. This is a significant advance in comparison with existing criteria, which allows pores to be more and more enclosed by solid particles as merging progresses; as a result, over-merging of tetrahedra can be avoided. We determined the size of each constriction shared by two adjacent pores by defining the largest empty sphere that can pass through the void space between their common solid particles.

The new criterion makes use of a user-specified value $\gamma^{\text{th}}$ for the admissible overlap between adjacent inscribed void spheres. As a consequence, pore sizes and constriction sizes depend on the chosen value of $\gamma^{\text{th}}$. Nonetheless, this dependency is substantially reduced in comparison with that found for the criterion of Shire and O'Sullivan [27]. In particular, the user can set this parameter to 0, which implies a strict separation between two adjacent pores, without leading to formation of complex pore entities.

We presented a comparison of the PSD and CSD given by the new criterion with those given by the criterion of Shire and O'Sullivan, both criteria with the same value of $\gamma^{\text{th}} = 0$, and the $L_1$ and $L_2$ criteria of Reboul et al. [21,22]. Uniformly graded (UG), gap-graded (GG) and widely graded (WG) samples at loose and dense states were considered for this comparison. It was shown that the PSDs and CSDs given by these four criteria differ greatly for the UG samples, particularly for the loose one. The PSDs and CSDs given by the new criterion are intermediate between those obtained with the criterion of Shire and O'Sullivan and the $L_1$ criterion but close to those given by the $L_2$ criterion. The differences between PSDs and CSDs given by these criteria are greatly reduced for the GG and WG samples, particularly for the dense ones. More interestingly, the four different criteria result in almost the same mode of the CSD.

It is worth mentioning that the pore space in granular materials is very complex and difficult to characterize. Therefore, any method used to extract this pore space suffers from an inherent subjectivity. Nevertheless, the new merging criterion presented in this paper allows us to mitigate this subjectivity and remediate the drawbacks of the criteria proposed by Shire and O'Sullivan and by Reboul et al. More interestingly, the CSD given by the new criterion is close to that given by the $L_2$ criterion and is bounded by those given by the $L_1$ criterion and the criterion of Shire and O'Sullivan as lower and upper limits, respectively. In particular, for gap-graded and widely graded materials, which are the most used soils for construction of earth-filled structures, the CSDs given by these four different criteria tend to converge, giving a good confidence in using this kind of approaches based on Delaunay triangulation to determine the CSD of granular filters. CSDs were used to estimate the controlling constriction sizes $D_c^*$ of the considered samples. The values of $D_c^*$

for the dense UG and WG samples were found to be consistent with the empirical rule $D_c^* < 0.2D_{15}$ widely used in the literature. For the dense GG sample, the estimated value of $D_c^*/D_{15}$ is higher than 0.2; however, it becomes significantly lower than 0.2 when the rattlers were removed from this sample. In addition, the CSDs of the dense samples were found to be significantly affected by the presence of these rattlers; however, their largest modal constriction diameters remain unchanged when the rattlers were removed.

The pore sizes and constriction sizes of a granular material depend on several factors, primarily on the particle size gradation and on the compactness, but also on the particle shape. Our upcoming work is to extend the new merging criterion presented in this paper to granular materials composed of non-spherical particles simulated with the DEM by clustering spherical balls. Furthermore, the sample generation procedure must be enhanced to eliminate unstable particles from numerical samples. The pore network extracted from a granular material by using the new merging criterion will be used to build a network model more physically sound than those based on the regular cubic network, with the aim of estimating the controlling constriction size of granular filters and assessing the susceptibility of granular soils to internal erosion. The performance of such a model can be validated against experimental tests.

**Acknowledgements** The authors would like to acknowledge Prof. Eric Vincens and Dr. Feda Seblany at Ecole Centrale de Lyon for valuable discussions about the $L_1$ and $L_2$ criteria and for having provided some data so that the authors could validate the implementation of these criteria in their own code. This work was partially supported by Cedre program of the French and Lebanese scientific cooperation.

## References

1. Al-Kharusi, A.S., Blunt, M.J.: Network extraction from sandstone and carbonate pore space images. Journal of Petroleum Science and Engineering **56**(4), 219–231 (2007)
2. Al-Raoush, R., Thompson, K., Willson, C.: Comparison of network generation techniques for unconsolidated porous media. Soil Science Society of America Journal **67**(6), 1687–1700 (2003)
3. Catalano, E.: A pore–scale coupled hydromechanical model for biphasic granular media. application to granular sediment hydrodynamics. Ph.D. thesis, Université de Grenoble (2012)
4. Chang, D.S., Zhang, L.M.: Extended internal stability criteria for soils under seepage. Soils and Foundations **53**(4), 569–583 (2013)
5. Csardi, G., Nepusz, T., et al.: The igraph software package for complex network research. InterJournal, Complex Systems **1695**(5), 1–9 (2006). URL https://igraph.org
6. Das, N.: Modeling three-dimensional shape of sand grains using discrete element method. Ph.D. thesis, University of South Florida (2007)
7. Dong, H., Blunt, M.J.: Pore-network extraction from micro-computerized-tomography images. Physical Review E **80**(3), 036307 (2009)
8. Gao, S., Meegoda, J.N., Hu, L.: Two methods for pore network of porous media. International Journal for Numerical and Analytical Methods in Geomechanics **36**(18), 1954–1970 (2012)
9. Homberg, U., Baum, D., Prohaska, S., Kalbe, U., Witt, K.: Automatic extraction and analysis of realistic pore structures from CT data for pore space characterization of graded soil. In: Proceedings of 6th International Conference on Scour and Erosion (ICSE-6), pp. 345–352 (2012)

10. Indraratna, B., Raut, A.K., Khabbaz, H.: Constriction-based retention criterion for granular filter design. Journal of Geotechnical and Geoenvironmental Engineering **133**(3), 266–276 (2007)
11. Kenney, T., Chahal, R., Chiu, E., Ofoegbu, G., Omange, G., Ume, C.: Controlling constriction sizes of granular filters. Canadian Geotechnical Journal **22**(1), 32–43 (1985)
12. Kenney, T., Lau, D.: Internal stability of granular filters. Canadian Geotechnical Journal **22**(2), 215–225 (1985)
13. Kenney, T., Lau, D.: Internal stability of granular filters: Reply. Canadian Geotechnical Journal **23**(3), 420–423 (1986)
14. Lafleur, J., Mlynarek, J., Rollin, A.L.: Filtration of broadly graded cohesionless soils. Journal of Geotechnical Engineering **115**(12), 1747–1768 (1989)
15. Li, Z., Wang, Y., Chow, J., Su, Z., Li, X.: 3D pore network extraction in granular media by unifying the Delaunay tessellation and maximal ball methods. Journal of Petroleum Science and Engineering **167**, 692–701 (2018)
16. van der Linden, J.H., Sufian, A., Narsilio, G.A., Russell, A.R., Tordesillas, A.: A computational geometry approach to pore network construction for granular packings. Computers & Geosciences **112**, 133–143 (2018)
17. Lindow, N., Baum, D., Hege, H.C.: Voronoi-based extraction and visualization of molecular paths. IEEE Transactions on Visualization and Computer Graphics **17**(12), 2025–2034 (2011)
18. Locke, M., Indraratna, B., Adikari, G.: Time-dependent particle transport through granular filters. Journal of Geotechnical and Geoenvironmental Engineering **127**(6), 521–529 (2001)
19. Marot, D., Rochim, A., Nguyen, H.H., Bendahmane, F., Sibille, L.: Assessing the susceptibility of gap-graded soils to internal erosion: proposition of a new experimental methodology. Natural Hazards **83**(1), 365–388 (2016)
20. O'Sullivan, C., Bluthé, J., Sejpar, K., Shire, T., Cheung, L.: Contact based void partitioning to assess filtration properties in DEM simulations. Computers and Geotechnics **64**, 120–131 (2015)
21. Reboul, N., Vincens, E., Cambou, B.: A statistical analysis of void size distribution in a simulated narrowly graded packing of spheres. Granular Matter **10**(6), 457–468 (2008)
22. Reboul, N., Vincens, E., Cambou, B.: A computational procedure to assess the distribution of constriction sizes for an assembly of spheres. Computers and Geotechnics **37**(1-2), 195–206 (2010)
23. Schuler, U.: Scattering of the composition of soils - an aspect for the stability of granular filters. In: Geofilters, vol. 96, pp. 21–34. Bitech Publications, Montreal (1996)
24. Seblany, F.: Filter criterion for granular soils based on the constriction size distribution. Ph.D. thesis, Ecole Centrale de Lyon (2018)
25. Seblany, F., Homberg, U., Vincens, E., Winkler, P., Witt, K.: Merging criteria for defining pores and constrictions in numerical packing of spheres. Granular Matter **20**(3), 37 (2018)
26. Sherard, J.L., Dunnigan, L.P., Talbot, J.R.: Basic properties of sand and gravel filters. Journal of Geotechnical Engineering **110**(6), 684–700 (1984)
27. Shire, T., O'Sullivan, C.: Constriction size distributions of granular filters: a numerical study. Géotechnique **66**(10), 826–839 (2016)
28. Shire, T., O'Sullivan, C.: A network model to assess base-filter combinations. Computers and Geotechnics **84**, 117–128 (2017)
29. Silin, D., Jin, G., Patzek, T.: Robust determination of the pore space morphology in sedimentary rocks. Journal of Petroleum Technology **56**(5), 69–70 (2004)
30. Silveira, A.: An analysis of the problem of washing through in protective filters. In: Proceedings of the sixth international conference on soil mechanics and foundation engineering, vol. 2, pp. 551–555 (1965)
31. Sufian, A., Russell, A., Whittle, A., Saadatfar, M.: Pore shapes, volume distribution and orientations in monodisperse granular assemblies. Granular Matter **17**(6), 727–742 (2015)
32. The CGAL Project: CGAL User and Reference Manual, 4.14.1 edn. CGAL Editorial Board (2019). https://doc.cgal.org/4.14.1/Manual/packages.html
33. V. Šmilauer and others: Yade Documentation 2nd ed. The Yade Project (2015). DOI 10.5281/zenodo.34073. http://yade-dem.org/doc/

34. Vincens, E., Witt, K., Homberg, U.: Approaches to determine the constriction size distribution for understanding filtration phenomena in granular materials. Acta Geotechnica **10**(3), 291–303 (2015)